Characterization and catalytic application of homogeneous nano-composite oxides ZrO_2–Al_2O_3

Guoran Li, Wei Li, Minghui Zhang, Keyi Tao*

Institute of New Catalytic Materials Science, College of Chemistry, Nankai University, Tianjin 300071, China

Abstract

A series of ZrO_2–Al_2O_3 composite oxides with different ZrO_2 contents was prepared by means of a chemical precipitation method using $ZrOCl_2 \cdot 8H_2O$ and pseudoboehmite as starting materials. The structures of the samples have been investigated by powder X-ray diffraction (XRD) and transmission electron micrography (TEM), with thermogravimetry differential thermal analysis (TG-DTA and DTG) combined. The results showed that the synthesized materials consisted of ZrO_2 and Al_2O_3 nanosized particles and they existed as amorphous phase in the samples with insufficient contents of ZrO_2. The surface areas (S_{BET}), the pore volumes and the pore distributions were measured by nitrogen adsorption method, and a regular correlation between the pore distributions and contents of ZrO_2 was observed. NH_3-temperature programmed desorption (NH_3-TPD) was used to characterize the surface acidic properties of the samples. The investigation by X-ray photoelectron spectroscopy (XPS) indicated that there were interactions between ZrO_2 and Al_2O_3 in the composite oxides. The synthesized ZrO_2–Al_2O_3 samples were purposively used as the supports for hydrodesulfurization (HDS) process. The sulfided CoMo/ZrO_2–Al_2O_3 catalysts were tested in the HDS reaction of dibenzothiophene (DBT), and the results showed that the sulfided CoMo catalysts supported on the composite oxide with a suitable ZrO_2 content performed a higher HDS activity than that supported on alumina.

1. Introduction

Hydrodesulfurization (HDS) of feedstock has been an indispensable reaction of produce clean fuels. Alumina-supported catalysts based on sulfided molybdenum promoted by Co or Ni are commonly used as HDS catalysts in the petroleum industry [1]. Recently, increasing environmental pressures and economical reasons have pointed out the necessity to develop new hydrotreating catalysts with enhanced properties. As one of the methods for improving the catalyst, modifying the nature of supports by addition of other materials such as TiO_2 [2], MCM-41 [3] and ZrO_2, etc. [4,5] has been considerably researched.

Among the mixed oxides used as HDS catalytic supports, ZrO_2–Al_2O_3 has received greater interest due to the unique properties of ZrO_2: to sustain acidic and basic sites, and to possess high thermal stability [6,7]. However, unlike TiO_2–Al_2O_3 system that has been studied extensively

and thoroughly because of its commercial prospects [8,9], the preparation and the properties of ZrO_2–Al_2O_3 as catalytic supports have not sufficiently been investigated yet. Mochida and coworkers [5] prepared zirconia–alumina supports by kneading pseudoboehmite powder and zirconia hydroxide powder with 3.2% HNO_3 and investigated the HDS of dibenzothiophene (DBT) on sulfided CoMo/ZrO_2–Al_2O_3 catalysts. In result, CoMo/ZrO_2–Al_2O_3 catalyst had lower activity for HDS of DBT than CoMo/Al_2O_3. ZrO_2–Al_2O_3 mixed oxides were also prepared by hydrolyze of alkoxides in which zirconium propoxide and aluminum isopropoxide were used, but their catalytic application was not reported [10].

In the present research, $ZrOCl_2 \cdot 8H_2O$ and pseudoboehmite with a high surface area and wide pores were used as starting materials, a series of ZrO_2–Al_2O_3 composite oxides with variable proportions between ZrO_2 and Al_2O_3 was prepared by the chemical precipitation method, resumptively, a precipitator was added into the mixed system containing alumina hydrate and $ZrOCl_2 \cdot 8H_2O$ aqueous solution. The morphological structures, the textural properties and the surface acidities of the as-prepared samples

* Corresponding author. Tel.: +86 22 2350 0027;
fax: +86 22 2350 0027.
E-mail address: kytao@nankai.edu.cn (K. Tao).

were investigated. Interestingly, the components of the as-prepared ZrO_2–Al_2O_3 composite oxides were dispersed in a homogenous way, in particular, their particles were of nanometric size. Furthermore, the composite oxides showed some specific properties differing from alumina or zirconia, e.g. the surface acidities. Finally, the ZrO_2–Al_2O_3 composite oxides were used as the supports in the HDS reaction of DBT. The sulfided CoMo catalysts supported on the composite oxide with a suitable ZrO_2 content performed a higher HDS activity than that supported on alumina.

2. Experimental

2.1. Preparation of the nano-composite oxides

The preparation of ZrO_2–Al_2O_3 supports employed the following procedure. Pseudoboehmite and deionized water were mixed with vigorous stirring, and then $ZrOCl_2 \cdot 8H_2O$ aqueous solution with a proper concentration was dripped into the system with a speed of 2 ml/min. When the liquid system was homogeneous, ammonia solution was slowly added until the system was solidified suddenly. The solid was thoroughly washed with deionized water until no chloride ions could be detected with $AgNO_3$ solution in the filtrate, and then washed with ethanol for three times. After that, the solid was made into stick form and dried in an atmosphere oven at 353 K over night and then dried at 393 K for 3 h. Finally, the dried solids were calcined at 823 K for 4 h in open-air atmosphere. Two kinds of methods were employed to prepare pure ZrO_2. One was the same as the preparation of the composite oxides excluding pseudoboehmite, and the product was analyzed by XRD. The other was from the reference [11] and the analysis results of XRD and FT-Raman showed that the ZrO_2 was pure tetragonal phase. In this work, the pure tetragonal ZrO_2 would be compared with the composite oxides in the subsequent characterizations. Al_2O_3 was directly obtained by calcining pseudoboehmite at 823 K. The symbols of the samples and their components are listed in Table 1.

2.2. Characterization of the nano-composite oxides

X-ray diffraction (XRD) patterns were recorded in the range $5° \leq 2\theta \leq 80°$ in a D/max-2500 diffractometer, using Cu Kα radiation ($\lambda = 1.5418$ Å) and a goniometer speed of 8°/min.

Thermogravimetry differential thermal analysis (TG-DTA) was carried out in a Rigaku Standard TG-DTA system with a temperature range 298–1073 K at a heating rate of 20 K/min. γ-Al_2O_3 was used as reference substance. The derivative thermogravimetry (DTG) profiles were obtained from TG profiles by derivation calculus.

Transmission electron microscopy (TEM) and selected area electron diffraction (SAED) were performed in a Philips EM400ST electron microscope. In order to observe possible crystal lattices of the samples, a TECNAI F20 transmission electron microscope with an acceleration voltage of 200 kV was also employed.

The BET surface areas (S_{BET}), the pore volumes and the pore diameter distributions were measured by N_2 adsorption at 77 K using a Micrometeritics ASAP 2010 apparatus. S_{BET} measurements were performed using a five-point BET method. The BJH method was applied to determine the pore diameter distributions.

The surface acidities of the samples were measured by NH_3-temperature programmed desorption (NH_3-TPD). TPD experiments were carried out in a self-established vacuum TPD characterization system equipped with a thermal conductivity detector (TCD), which had been confirmed dependable. The TPD curves were fitted according to Gauss functions using Origin7.0.

X-ray photoelectron spectroscopy (XPS) measurements were performed at room temperature in a Perkin-Elmer PHI (4) 5300ESCA analyzer. The work pressure was under 10^{-7} Pa. Photoelectrons were excited using the unmonochromatized Mg Kα line at 1253.6 eV. A pass energy of 89.45 eV was used to obtain the survey spectra and 35.75 eV was used for the high-resolution, multiregion scans. Due to the charging problem of the insulating samples the binding energies values were referenced to the C 1s line at 284.8 eV arising from the inadvertent carbon contamination. The uncertainty in the determination of the binding energy values was estimated to be about 0.2 eV.

2.3. Catalytic applications of the nano-composite oxides

Considering the surface areas of the as-prepared composite oxides, only ZA10, ZA20 and ZA40 were used as catalytic supports. The sulfided CoMo/ZA catalysts were

Table 1
S_{BET}, pore volumes, pore diameter distributions and ZrO_2 content of the samples

Sample	S_{BET} (m^2/g)	Pore volume (cm^3/g)	Average pore diameter (nm)	ZrO_2 content (wt.%)
Al_2O_3	313	1.05	13.4	–
ZA10	217	0.45	8.1	12.1
ZA20	265	0.41	6.2	21.4
ZA40	161	0.20	4.9	41.0
ZA80	95	0.27	11.2	80.0
ZrO_2	51	0.34	26.7	100

prepared by a conventional route including impregnation, drying, calcination and sulfuration [3]. Also, CoMo/Al$_2$O$_3$ was prepared by the same method. The loading amount of CoO and MoO$_3$ was 2 and 15 wt.%, respectively. The HDS reaction of DBT in decalin (0.5 wt.% DBT) was carried out in a continuous feed reactor. The operation employed the following conditions: H$_2$ pressure 3.0 MPa, H$_2$ flow rate 200 ml/min, LHSV 15 h^{-1}, temperature 513–593 K. The liquid samples were collected at an hour's interval and analyzed by gas chromatography with a flame ionization detector (FID) and a commercial capillary column OV101. The conversion of DBT was used to evaluate the activity of catalysts.

3. Results and discussion

3.1. XRD

The XRD patterns of the samples are shown in Fig. 1. It is evident that the Al$_2$O$_3$ obtained by calcination of pseudoboehmite at 823 K presented the crystalline γ-Al$_2$O$_3$ structure. As compared with Al$_2$O$_3$, the composite oxides ZA10, ZA20 and ZA40 showed a broadened peak at $2\theta = \sim30°$, and the intensity of the peak increased with increasing zirconia contents. The broadened peak was attributed to the tetragonal phase zirconia in the literature [10], but it was also considered as an appearance of amorphous zirconia [7]. Here it has further been identified by SAED and HRTEM (shown in the later paragraph) that ZrO$_2$ was amorphous in the above-mentioned samples. However, the XRD pattern of ZA80 showed sharp peaks at $2\theta = 30.2°$ and 50.3°, which was obviously the trait of tetragonal zirconia. No peak identifying monoclinic zirconia ($2\theta = 28.1°$)

in the pattern of ZA80 was observed, namely, ZrO$_2$ component in ZA80 sample was only tetragonal phase (due to poor intensity, the peaks of Al$_2$O$_3$ were not seen in the pattern). On the other hand, the pattern of the pure ZrO$_2$ that was prepared by the chemical precipitation method revealed that the sample was chiefly composed of monoclinic zirconia, with a small quantity of tetragonal zirconia. These results showed that the metastable tetragonal ZrO$_2$ were more stable at room temperature owing to the incorporation of Al$_2$O$_3$. In general, it seems that the co-existence of ZrO$_2$ and Al$_2$O$_3$ in the composite samples can affect the intrinsic structure each other. This may be due to the formation of a phase segregation between alumina and zirconia as a result of the homogenous dispersion, which will further be illustrated by the TG-DTA.

Considering the comparison between ZrO$_2$ and ZrO$_2$–Al$_2$O$_3$ composite oxides especially ZA80, pure tetragonal ZrO$_2$ was used in the TG-DTA, N$_2$ adsorption, TPD and XPS.

3.2. TG-DTA

The dried samples (not calcined) were analyzed by TG-DTA (Fig. 2). Clearly, all samples but ZrO$_2$ had endothermal peaks about 370 and 545 K corresponding to the dehydration processes and the loss of hydroxyls, respectively. ZrO$_2$ had no obvious dehydration behavior at 370 K, perhaps because ZrO$_2$ provided wider pores than others (Table 1), which made it easier to be dried fully in the same conditions. It was also noticed that ZrO$_2$ had not a endothermal peak about 545 K; on the contrary, it showed unconspicuous exothermic behavior around 538 K that could only be assigned to a certain change in the structure of ZrO$_2$. The exothermic peak covered the peak brought by the removal of hydroxyl in DTA curves, but the weight loss in this temperature range illuminated the loss of the hydroxyl. The exothermic behavior at 773 K was attributed to crystallization of ZrO$_2$. In the case of Al$_2$O$_3$, the exothermic peak at 808 K corresponded to the formation of γ-Al$_2$O$_3$. However, these crystallization processes
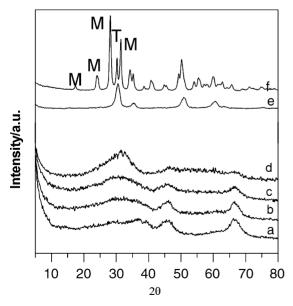

Fig. 1. Powder X-ray diffraction patterns of: (a) Al$_2$O$_3$; (b) ZA10; (c) ZA20; (d) ZA40; (e) ZA80; (f) ZrO$_2$. M and T mean monoclinic ZrO$_2$ and tetragonal ZrO$_2$, respectively. The patterns in (e) and (f) underwent a 0.2-fold *Y*-scale reduction.
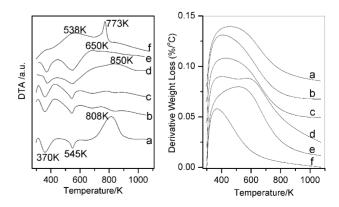

Fig. 2. DTA and DTG curves of: (a) Al$_2$O$_3$; (b) ZA10; (c) ZA20; (d) ZA40; (e) ZA80; (f) ZrO$_2$.

of ZrO_2 and Al_2O_3 were not seen clearly in the composite oxides. ZA10 and ZA20 showed approximate DTA curves and there was no clear exothermic or endothermal process over 600 K. On the other hand, ZA80 began to release heat from 650 K, which could be assigned to the formation of tetragonal ZrO_2 (perhaps, crystallization of γ-Al_2O_3 was included). In the case of ZA40, there was an exothermic process beginning from 850 K that was higher than that of ZA80. In order to confirm the phase transition, ZA40 calcined at 923 K was examined by XRD (Fig. 3). The presence of the tetragonal ZrO_2 character peaks in the pattern effectively indicated that the exothermic process of ZA40 corresponded to ZrO_2 crystallization.

The phenomena support the following deduction. In ZA10 and ZA20, ZrO_2 was dispersed in the alumina matrix so adequately that it could not form crystalline structure; simultaneously, the existence of ZrO_2 successfully restrained the crystallization of Al_2O_3. Both ZrO_2 and Al_2O_3 were amorphous. With the increase of ZrO_2 contents, ZrO_2 particles gained more and more chances to congregate and crystallize. ZA40 and ZA80 began crystallization at 850 and 650 K, respectively.

Combining the results of XRD, it can be considered that either of the two components, ZrO_2 and Al_2O_3, were fully dispersed into the matrix of the other one in a homogenous way. This kind of dilution led to a new nano-composite structure with amorphous components differing from ZrO_2 or Al_2O_3.

3.3. TEM and SAED

As a representative, the TEM photograph (Fig. 4) and the corresponding SAED pattern (the inset in Fig. 4) of ZA40 are shown. It can be observed from the TEM photograph that ZA40 consisted of fine particles with a size of $\sim$10 nm, and these particles could not be distinguished between ZrO_2 and Al_2O_3. In the SAED pattern, there was no diffraction spots or diffraction rings caused by crystalline ZrO_2, which showed that ZrO_2 in ZA40 existed in an amorphous structure. Furthermore, a HRTEM observation indicated that no
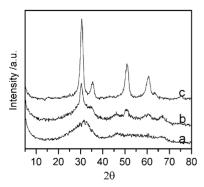

Fig. 4. TEM photograph and SAED pattern (the inset) of ZA40.

Fig. 3. XRD patterns of ZA40 calcined at (a) 823 K; (b) 923 K; (c) and tetragonal ZrO_2.

space lattices of crystalline ZrO_2 was found, while the lattice spacing could clearly been observed in the supported ZrO_2 micro crystal [12].

3.4. N_2 adsorption

The surface areas (S_{BET}), the pore volumes and the pore distributions of the samples are summarized in Table 1. The S_{BET} of ZrO_2 was only 51 m^2/g, whereas that of Al_2O_3 was up to 313 m^2/g. From ZA20 to ZrO_2, the S_{BET} decreased gradually while the contents of ZrO_2 increased. However, ZA10 provided a lower S_{BET} than ZA20. Possibly, it was due to the different particle size of ZrO_2 in the pores of Al_2O_3. The pore volumes and the average pore diameters presented the same trend. The pore volumes decreased rapidly by the incorporation of ZrO_2 and the average pore sizes diminished clearly compared with those of Al_2O_3. And ZA40 had the smallest pore volume and pore size. On the other hand, the pore volumes and the pore diameters of the samples (from ZrO_2 to ZA40) turned to diminishment by the incorporation of Al_2O_3 into ZrO_2.

The pore diameter distribution curves of the samples are shown in Fig. 5. The pores of Al_2O_3 were distributed in the relatively wide range (2–40 nm), while the pores of ZA10, ZA20 and ZA40 were in the range 2–10 nm. From ZA10 to ZA40, the maximum of the pore size distribution curves had a left shift, namely, wider diameter pores disappeared. On the other hand, ZrO_2 had larger pore size and wider distribution, whose pores were distributed diffusely in the range 4–100 nm. However, ZA80 had hardly any pore >20 nm. These results showed that the new textural features differing from those of Al_2O_3 or ZrO_2 were formed in the synthesis of ZrO_2–Al_2O_3 composite oxides.
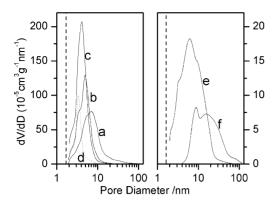
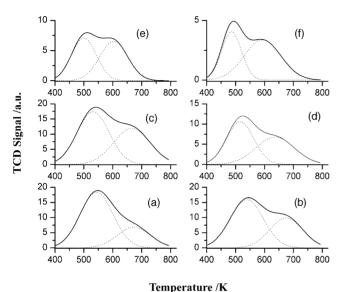Fig. 5. The pore diameter distribution curves of: (a) Al_2O_3; (b) ZA10; (c) ZA20; (d) ZA40; (e) ZA80; (f) ZrO_2.

Fig. 6. NH_3-TPD profiles of: (a) Al_2O_3; (b) ZA10; (c) ZA20; (d) ZA40; (e) ZA80; (f) ZrO_2.

3.5. NH_3-TPD

The TPD curves for NH_3 evolution from the different oxides are shown in Fig. 6. Table 2 summarizes the temperatures and the area percentages of NH_3 desorption peaks, as well as the total NH_3 adsorption amounts and densities on the samples. Two desorption peaks based on Gaussian fit can be observed in all the cases: one was in the temperature
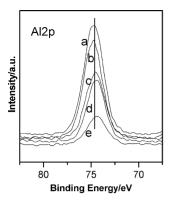
range 490–550 K, and the other was in the range 590–680 K, which corresponded to weak and strong acid sites, respectively [13]. It can be found that the area percentage of the peak II gradually increased, while the T_{m2} decreased from Al_2O_3 to ZrO_2, with ZrO_2 content increasing. Obviously, the samples containing ZrO_2 had more strong acid sites than the pure alumina. Corresponding to a higher desorption temperature, these new acidic sites had stronger intensity than those of ZrO_2. This should be attributed to the interaction between ZrO_2 and Al_2O_3, e.g. the formation of Zr–O–Al bonds [14]. The interaction will further be proved by XPS analysis. Also, the increase of acid sites was observed from the change of the supports' acid amounts that depend on S_{BET} and the acid site density. Though ZA10 and ZA20 had lower S_{BET} than Al_2O_3, their surface acid amounts were more than that of Al_2O_3. This result was due to the increasing acid site densities, whereas the diminishment of acid amounts from ZA40 to ZrO_2 was because of the drastic decrease of S_{BET}. According to Table 2, Al_2O_3 had the lowest acid site density, while ZrO_2 provided the highest one. From ZA10 to ZA80, a unconspicuous climbing trend for the acid site densities could be observed. In fact, the acid amount was usually paid more attention in the practical application of supports. The research results showed the possibility of tuning the surface acidity of ZrO_2–Al_2O_3 supports by modifying ZrO_2 contents.

3.6. XPS

XPS has been used to investigate the binding energies of the different element and Zr/Al surface atomic ratio of the samples. Fig. 7 shows the XPS spectra of Al 2p and Zr 3d of the samples and Table 3 lists the BE values of Al 2p, Zr 3d and O 1s. As it was seen, though ZA10, ZA20 and Al_2O_3 had the same BE of Al 2p, ZA40 showed a BE shift to the lower value, and that the similar shift became more obvious in the case of ZA80. The phenomena can be understood that more ZrO_2 content conduced to a clearer effect on Al_2O_3. Similarly, in the spectra of Zr 3d, ZA80, ZA40 and ZrO_2 had the same BE, while ZA10 and ZA20 showed higher binding energies. In addition, the trough between Zr $3d_{5/2}$ peak and Zr $3d_{3/2}$ peak became ambiguous and the left shoulder of Zr $3d_{3/2}$ peak of ZA20 became wide in the spectra of Zr 3d for ZA10 and ZA20. In the case of the BE of O 1s, the value

Table 2
Surface acidic features of the samples measured by NH_3-TPD

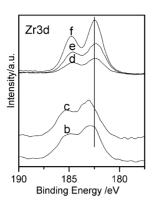| Sample	Peak I		Peak II		Total amount of acid sites (mmol/g)	Acid sites density (numbers/nm^2)
	T_{m1} (K)	Percentage of area (%)	T_{m2} (K)	Percentage of area (%)		
Al_2O_3	544	75	673	25	0.82	1.58
ZA10	539	62	675	38	0.89	2.47
ZA20	532	57	670	43	1.00	2.27
ZA40	517	53	637	47	0.73	2.73
ZA80	500	49	603	51	0.45	2.86
ZrO_2	490	39	593	61	0.31	3.68

Fig. 7. Al 2p and Zr 3d XP spectra of: (a) Al_2O_3; (b) ZA10; (c) ZA20; (d) ZA40; (e) ZA80; (f) ZrO_2. The spectra in (a) and (b) underwent a six-fold Y-scale magnification.
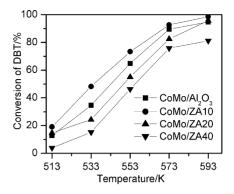

Fig. 8. Conversion of DBT performed on the different catalysts. H_2 pressure 3.0 MPa, H_2 flow rate 200 ml/min, LHSV $15 h^{-1}$.

of Al_2O_3 was higher than that of ZrO_2. In general, it can be considered that, in the composite samples, there was a certain interaction between Zr and Al such as Zr–O–Al [14]. The results are consistent with the research of Su et al. [15].

The quantitative analysis results by XPS are presented in Table 3. The Al/Zr calculated values were calculated from the ZrO_2 contents in the composite oxides, which could reflect the bulk components of the samples. It is observed from Table 3 that the analysis results of the composite oxides were in agreement with their calculated values well, which suggested a uniform composition both in the surface and the bulk of the composite oxides.

3.7. Catalytic application

The conversions of DBT were used to indicate activities of the catalysts. Fig. 8 shows the conversions of DBT on sulfided CoMo catalysts supported on the different supports: ZA10, ZA20, ZA40 and Al_2O_3 at various reaction temperatures. Obviously, the activities of all catalysts increased when the reaction temperature increased form 513 to 593 K. At the same temperature, the catalyst supported on ZA10 performed a higher catalytic activity than that supported on alumina. However, CoMo/ZA20 and CoMo/ZA40 showed lower catalytic activities, which was possible related to their incompetent textural properties; namely, the highest HDS activity of the catalysts required an optimum content

of ZrO_2 in the composite supports which was 12.1 wt.% in our research.

It is well known that the nature of supports, especially the surface properties, is one of the most important factors affecting activities of catalysts. In this research, compared with alumina, the composite oxides containing ZrO_2 provided much different traits due to the interaction ZrO_2 and Al_2O_3. As a potential catalytic support, ZA10 had the specific texture and the unique surface acid properties that were different from either alumina or zirconia. These specific characters might be more suitable to for HDS catalysts than those of Al_2O_3. For example, they might induce the variation in dispersion and morphology of active component and possible interactions between metals and supports which may change the activity and/or selectivity of the catalysts. This will be researched in the subsequent works.

4. Conclusions

ZrO_2–Al_2O_3 nano-composite oxides used as the catalytic supports for DBT HDS reaction were prepared. In the samples calcined at 823 K, ZrO_2 presented as amorphous phase in the composite oxides with low ZrO_2 contents (ZA10, ZA20 and ZA40), but tetragonal phase in the ZA80 containing 80 wt.% ZrO_2. The composite oxides consisted of nano-sized particles and provided the new texture features differing from that Al_2O_3 or ZrO_2. The acid amounts and the pore distribution of the supports could be controlled by modifying amounts of ZrO_2. The sulfided CoMo catalyst supported on the ZA10 with 12.1 wt.% ZrO_2 content performed a higher HDS activity of DBT than the sulfided CoMo/Al_2O_3.

Table 3
XPS data of the synthesized samples

Sample	Binding energy (eV)			Al/Zr	
	Al 2p	Zr 3d	O 1s	Calculated value	XPS
Al_2O_3	74.8	–	531.7	∞	∞
ZA10	74.7	182.9	531.7	12.8	12.7
ZA20	74.7	183.1	531.6	8.9	8.7
ZA40	74.5	182.4	531.3	3.0	3.4
ZA80	74.3	182.4	530.5	0.7	0.6
ZrO_2	–	182.5	530.3	0	0

References

[1] H. Topsøe, B.S. Clausen, F.E. Massoth, Hydrotreating Catalysis Science and Technology, vol. 11, Springer, Berlin, 1996.

[2] Y. Araki, K. Honna, H. Shimada, J. Catal. 207 (2002) 361.

[3] J. Ramirez, R. Contreras, P. Castillo, T. Klimova, R. Zarate, R. Luna, Appl. Catal. A 197 (2000) 69.

[4] S. Damyanova, M.A. Centeno, L. Petrov, P. Grange, Spectrochim. Acta A 57 (2001) 2495.

[5] E. Lecrenay, K. Sakanishi, I. Mochida, T. Suzuka, Appl. Catal. A 175 (1998) 237.

[6] V. Quashning, J. Deutsch, P. Druska, H.J. Niclas, E. Kemnitz, J. Catal. 177 (1998) 164.

[7] S. Damyanova, P. Grange, B. Delmon, J. Catal. 168 (1997) 421.

[8] S.K. Maity, J. Ancheyta, L. Soberanis, F. Alonso, M.E. Llanos, Appl. Catal. A 244 (2003) 141.

[9] M.P. Borque, A. Lopez-Agudo, E. Olguin, M. Vrinat, L. Cedeno, J. Ramirez, Appl. Catal. A 180 (1999) 53.

[10] T. Klimova, M.L. Rojas, P. Castillo, R. Contreras, J. Ramirez, Micropor. Mesopor. Mater. 20 (1998) 293.

[11] G.K. Chauah, Catal. Today, 49 (1999) 131.

[12] M.A. Schofield, C.R. Aita, P.M. Rice, M. Gajdardziska-Josifovska, Thin Solid Films 326 (1998) 106.

[13] J. Meusinger, H. Vinek, J.A. Lercher, J. Mol. Catal. 87 (1994) 263.

[14] M. Moran-Pineda, S. Castillo, T. Lopez, R. Gomez Cordero-Borboa, O. Novaro, Appl. Catal. B 21 (1999) 79.

[15] G. Su, W. Zhang, H. Yang, Chin. J. Catal. 16 (1995) 145.